JCTC Journal of Chemical Theory and Computation

Article

pubs.acs.org/JCTC

Comparison of Molecular and Primitive Solvent Models for Electrical Double Layers in Nanochannels

Jonathan W. Lee, Jeremy A. Templeton,* Kranthi K. Mandadapu, and Jonathan A. Zimmerman

Sandia National Laboratories, Livermore, California

Supporting Information

ABSTRACT: In a recent article (Lee et al. *J. Comput. Theor. Chem.*, **2012**, *8*, 2012−2022.), it was shown that an electrolyte solution can be modeled in molecular dynamics (MD) simulations using a uniform dielectric constant in place of a polar solvent to validate Fluid Density Functional Theory (f-DFT) simulations. This technique can be viewed as a coarse-grained approximation of the polar solvent and reduces computational cost by an order of magnitude. However, the consequences of replacing the polar solvent with an effective permittivity are not well characterized, despite its common usage in f-DFT, Monte Carlo simulation, and Poisson−Boltzmann theory. In this paper, we have examined two solvent models of different fidelities with MD simulation of nanochannels. We find that the models produce qualitatively similar ion density profiles, but physical quantities such as electric field, electric potential, and capacitance differ by over an order of magnitude. In all cases, the bulk is explicitly modeled so that surface properties can be evaluated relative to a reference state. Moreover, quantities that define the reference state, such as bulk ion density, bulk solvent density, applied electric field, and temperature, are measurable, so cases with the same thermodynamic state can be compared. Insights into the solvent arrangement, most of which can not be determined from the coarse-grained model, are drawn from the model with an explicitly described polar solvent.

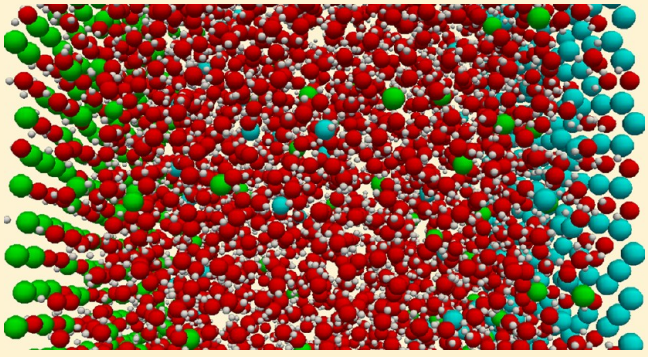

INTRODUCTION

Characterizing the behavior of an electrolyte fluid confined between solid surfaces is important for research and technologies ranging from energy storage[1−3] to microfluidics-based biology.[4,5] According to classical theories, ions near a charged wall form an electric double layer (EDL),[6] which is comprised of the Stern layer, a mostly immobile layer of counterions closest to the wall, and the diffuse layer, a region of decaying electric potential where both counterion and coion species can be present. The characteristic length scale of the EDL is referred to as the Debye length:

$$\lambda_D = \sqrt{\frac{\varepsilon k_B T}{2 n^o e^2}} \tag{1}$$

where k_B is the Boltzmann constant, T is the temperature, n^o is the bulk molarity, and e is the elementary charge. The permittivity of the medium, ε, is the product of the vacuum permittivity, ε_o, and the relative permittivity, ε_r. It has been shown that as the Debye length approaches molecular length scales, the Classical Poisson−Boltzmann (PB) theory breaks down.[7,8] The continuum-based PB theory has been widely used in the modeling of electro-osmotic flow (EOF), electrochemical capacitors, etc.[9−15] While the theory is a reasonable approximation for low ion concentrations and low surface charges, finite particle sizes and atomic packing structures lead to inaccuracy.

In PB theory, ions pack near the wall according to the Boltzmann distribution with the corresponding surface potential. Ions are assumed to be infinitesimal in size, and particle interactions are assumed negligible. The first order approximation of the Boltzmann distribution is expressed as

$$n_+ = n_+^o \exp\left(\frac{-\phi e}{k_B T}\right) \quad \text{and} \quad n_- = n_-^o \exp\left(\frac{\phi e}{k_B T}\right) \tag{2}$$

where n is the molarity of the ion species, ϕ is the local value of the total electric potential (relative to the bulk value), and subscripts denote the sign of the ion charge. Note the distribution dictates that the counterion concentration decays monotonically away from the surface. However, in the case of atomistic simulations, atoms and ions will form a particular packing structure, which yields peaks and valleys in their density profiles.[8] As electrolyte concentrations and applied voltages increase, resolution of the density oscillations becomes increasingly important. In this regime, engineering based on PB theory becomes unfeasible. It should be noted that modified PB theories have been proposed which correct for finite packing.[16−21] While these provide density distributions that are much more physically reasonable, we will be exploring options that give a more explicit description of the equilibrium EDL state to gain a better understanding of atomistic and molecular effects.

Received: March 14, 2013

   dx.doi.org/10.1021/ct4002043 | *J. Chem. Theory Comput.* XXXX, XXX, XXX−XXX

To that end, simulation techniques such as Fluid Density Functional Theory (f-DFT), Monte Carlo (MC), and molecular dynamics (MD) may be used to elucidate double layer physics. For example, f-DFT has been utilized to calculate over a wide range of surface potentials and ionic concentrations.[7,8,22] The work of Tang et al.[22] in the early 1990s modeled 0.1 molar (M) and 1 M solutions with normalized surface charges ranging from 0.05 to 0.7. Nilson et al.[7] expanded on this work while studying EOF in nanochannels with simulations ranging from 1 mM to 1 M for normalized surface charges from 0.0 to 1.0. The advantage of these f-DFT calculations is that reference state properties (i.e., reference energy, bulk fluid density, and bulk ionic concentration) are all specified as boundary conditions.

However, f-DFT has theoretical and numerical difficulties simulating bonded molecules with angle constraints. As such, to our knowledge, there is no evidence of published f-DFT work using the molecular solvent model (MSM), where atomic constituents of each solvent molecule and solute ions are explicitly described as distinct atoms. Henderson et al.[23] used a symmetric dumbbell solvent model in f-DFT to approximate the effects of polar water. Alternatively, f-DFT has typically utilized the primitive model (PM),[24] the restricted primitive model (RPM),[25] and the three-component model (3CM)[22] in simulating such systems. PM describes the solvent material as a uniform, isotropic dielectric continuum, and therefore, it is not explicitly modeled. The RPM additionally restricts PM such that the two ionic species are the same size. The 3CM, a coarse-grained approximation of the MSM, simulates the solvent molecule as a charge-neutral atom. Typically, ions are also restricted in size as with RPM. It is with the 3CM technique that PB theory can clearly be shown to deviate from atomistic results.[7,8]

For even greater fidelity models, one can employ discrete atomistic simulations, such as MC and MD. The PM, RPM, and 3CM have been explored using MC simulation by Torrie and co-workers[26−29] and, more recently, by Lamperski and collaborators.[30,31] As with the f-DFT calculations, MC simulations show that the solvent material must be explicitly modeled to reveal more accurate ion density oscillations near the wall. This can then be used to define the condensed and diffuse layers. Here, the condensed layer refers to the region where the steric effects due to packing of ions are important,[32] and the diffuse layer refers to the region where PB theory is valid.

MD simulations have been used extensively as well to model the EDL and EOF at various molarities and surface charge densities.[38,12,13,15,33−40] With the exception of Freund,[12] Qiao and Aluru,[13] Kim and Darve,[15] and Lee et al.,[8] all cited MD simulations studied ion concentrations of 1−2 M (or the authors did not specify). One should be wary that some of these studies feature an isolated double layer where coions are not present, so direct comparisons between similar molarities can not be drawn and are not intended. Freund[12] reports a molarity of approximately 0.01 M. Qiao and Aluru[13] and Kim and Darve[15] have unspecified molarities, but both appear to be on the order of 0.1 M. The study by Lee et al.[8] ranged from 0.01 M to 1 M. Most of the cited studies have surface charges of approximately 0.1 C/m^2, with a few cases up to 0.32 C/m^2. At these low charge densities, PB theory still predicts a valid approximation of ion distributions barring the first monolayer. Prior to the formation of a second ion layer, the shape of the first ion peak combined with its long exponential tail gives the illusion of a Boltzmann distribution. However, divergence from PB theory is emphasized at higher surface charges, where subsequent ion layers are formed, and the illusion is broken. While these charge densities may be normal for EOF models, the push for increased charge storage in electrochemical devices demands a wider range of surface charges.

The 3CM has been used with f-DFT and MD to show deviations from PB theory at higher surface charges.[7,8] However, the assumption of a uniform dielectric constant in the 3CM is potentially problematic close to the surface. While MD studies of electrolyte solutions near electrified interfaces have been performed using both the 3CM[8,40] and MSM,[8,12,13,15,33−39] the consequence of the 3CM approximation has not been quantified.

In the current paper, the 3CM is compared against the higher fidelity MSM using various metrics, such as capacitance, spatial variations in density, electric field, and electric potential, and near-wall fluid structure. While the ionic density profiles show some qualitative agreement, closer inspection shows major discrepancies in surface properties relative to the reference state. We will also show that, even for low surface charges, the MSM produces results that cannot be reproduced by the 3CM. In the following section, we will describe the two MD models and how the simulations are performed. This is followed by the results section, in which the models are compared using an assortment of aforementioned metrics over a wide range of surface charges. The final section provides a brief summary.

COMPUTATIONAL DETAILS

MD simulations of an electrically charged nanochannel were performed with the LAMMPS software package[41] to compare the coarse-grained water model (3CM)[22] and the TIP3P water model (MSM)[42,43] over a range of surface charge densities. The simulation domain consists of a 1:1 electrolyte fluid bounded in the z-dimension by two substrate walls, which are positioned such that the EDLs do not overlap and a bulk region can be defined. Classically, EDL lengths are determined by the Debye lengths, which depend on the ionic molarity. For ease of computation, we only explore the 1 M case. Simulating concentrations near 1 M (at 300 K in water) simplifies the problem for MD considerably for two reasons. First, ion counts are large, allowing the statistics to converge much faster. Second, the Debye length from PB theory at 1 M is 3.08 Å, which is approximately one atomic diameter. Therefore, the simulation domain can be quite small while still maintaining the ability to resolve bulk properties.

Periodic boundary conditions are applied in the transverse directions with a cross-section of 5 nm × 5 nm. Atomic interactions among all species are modeled with the Lennard-Jones (LJ) potential[44] and Coulomb's law. The LJ potential is given by

$$E = 4\xi_{LJ}\left[\left(\frac{d_{LJ}}{r}\right)^{12} - \left(\frac{d_{LJ}}{r}\right)^{6}\right] \tag{3}$$

where ξ_{LJ} and d_{LJ} are the energy and length parameters associated with the pair potential, respectively. Simulations are performed at a nominal temperature of 300 K.

As discussed previously, we are interested in studying the 3CM and MSM. The 3CM is a coarse-grained solvent model where the molecule is treated as one electrically neutral atom. In general, polar solvent molecules will prevent oppositely charged ions from approaching too closely by forming a solvation shell. Setting the dielectric constant ϵ_r to 80[12,35] approximates this complex effect by reducing all Coulombic interactions by a factor of 80. Effectively, the energy well from the total interatomic potential (Coulombic plus LJ) is comparable to that of a solvated ion with this dielectric

dx.doi.org/10.1021/ct4002043 | J. Chem. Theory Comput. XXXX, XXX, XXX−XXX

constant. The MSM uses the TIP3P water model where there are three charge and mass carrier sites on each molecule, and only the oxygen site interacts via the LJ potential with other atoms and molecules. Charges on the hydrogen and oxygen atoms are fractional charges, and masses are obtained from the periodic table. Bonds and angles are held rigid using the SHAKE algorithm.[45] Aside from the hydrogen atoms, all atoms have the same atomic size as each other. The ions' masses are taken to be equivalent to the solvent mass for simplicity (note that the masses should not affect the equilibrium quantities we are interested in). In the case of the 3CM, the size of the solvent atom is the same as that of the MSM oxygen atom, and the mass is the same as the total water molecule. To model the substrate−fluid interaction, we use LJ 10−4−3 walls[46] (unstructured one-dimensional wall potentials), which are the result of integrating the LJ potential over planar sheets of wall atoms. The LJ 10−4−3 walls have the form:

$$E = 2\pi\xi_{LJ}\left[\frac{2}{5}\left(\frac{d_{LJ}}{r}\right)^{10} - \left(\frac{d_{LJ}}{r}\right)^{4} - \frac{\sqrt{2}\,d_{LJ}^{3}}{3(r + (0.61/\sqrt{2})d_{LJ})^{3}}\right] \quad (4)$$

The wall potential uses a cutoff of 3.5 times the corresponding d_{LJ}. A summary of simulation parameters is shown in Table 1.

Table 1. Atomistic Parameters for the 3CM and the MSM[a]

atom	mass (g/mol)	ξ_{LJ} (kJ/mol)	d_{LJ} (Å)	q (e)	ref
solvent (3CM)	18.0154	0.6364	3.188	0	42, 43
H (MSM)	1.008	0.0	0.0	+0.415	42, 43
O (MSM)	15.9994	0.6364	3.188	−0.830	42, 43
positive ion (3CM and MSM)	18.0154	0.6364	3.188	+1	42, 43
negative ion (3CM and MSM)	18.1054	0.6364	3.188	−1	42, 43
LJ 10−4−3 wall	N/A	13.035	3.188	N/A	N/A

[a]Apart from hydrogen (which does not interact via LJ), inter-species parameters are obtained by the Lorentz-Berthelot mixing rules:[51,52] geometric mean for ξ_{LJ} and arithmetic mean for d_{LJ}.

Equations of motion are integrated with the velocity−Verlet algorithm.[47,48] A time step of 0.5 fs is used. LJ and short-range Coulomb interactions both use a 13 Å cutoff radius. Long range Coulombics are computed using the PPPM algorithm[49] with slab geometry.[50]

MD systems are initialized according to the following procedure. Solvent (oxygen) atom and ion coordinates are randomly placed at body-centered cubic lattice sites. For the MSM cases, hydrogen atoms are placed in a random configuration around the oxygen atoms. The total number of solvent atoms is chosen such that the bulk solvent density targets that of water at standard temperature and pressure. Similarly, the number of ions is chosen such that the bulk molarity is targeted toward 1 M. Note that for MD simulations, bulk densities and molarities cannot be determined *a priori*, so iterations are required to reach the target conditions.

To model oppositely charged surfaces, a linear background electric field is applied to the system proportional to the surface charge density. The applied field should also be scaled by the appropriate permittivity value to compare identical thermodynamic states. All atom velocities are initialized to zero. The fluid box is equilibrated for one million timesteps to 300 K. A Nosé−Hoover[53−55] thermostat is used to regulate the temperature during equilibration. To avoid any local minima in the energy landscape, the system is annealed to 1000 K for one million timesteps, followed by a cooling step back to 300 K for two million timesteps.

After the system is equilibrated, thermostats are turned off to ensure the equilibrium statistics are not influenced by the thermostats. The system is allowed to relax for five million timesteps. The first one million timesteps after equilibration is considered transient, and the rest are confirmed to be steady state. Five permutations are performed for each surface charge case.

Spatially dependent particle concentrations are extracted for every species from the domain via an atomistic-to-continuum (AtC) coarse-graining method.[56] In this method, atomistic data is projected onto a one-dimensional (1-D) continuum mesh using piecewise linear basis functions. The resolution of the 1-D mesh is approximately 0.1 Å. Number density data at all nodes is collected every 250 fs to facilitate postprocessing. After removing transient data, the remaining data is time- and ensemble-averaged. Number density scaled by the atomic valence can be integrated once to get the z-component of the electric field and integrated twice to obtain the electric potential. Electric surface potential is determined by taking the difference between the electric potential evaluated at the fluid-wall interface and the electric potential evaluated in the bulk. The fluid-wall interface is defined to be a half molecular diameter from the origin of the LJ 10−4−3 potential. All bulk properties are measured from the center 7 Å of the domain.

RESULTS

Figure 1 is an overview of the model comparison. It shows computed electric surface potentials for the negative and positive walls as a function of the applied surface charge for a nominal molarity of 1 M. Both the 3CM and the MSM are overlaid on top of each other for comparison purposes. The inverse of this curve is typically used to find the capacitance of the double layer by taking its slope (specifically the capacitance

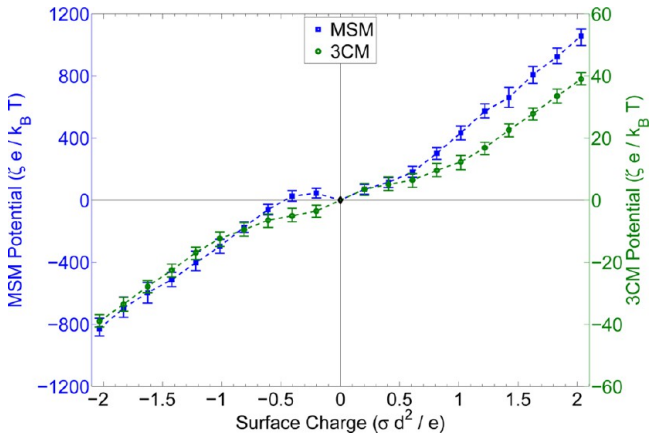

Figure 1. Electric potential relative to the bulk as a function of surface charge for the 3CM and MSM. The MSM results are plotted with blue squares on the left axis, and the 3CM results are plotted with green circles on the right axis. Minimum and maximum potentials observed in the course of the MD simulations are denoted by the error bars to estimate the uncertainty in those measurements. The inverse of the slope is the capacitance of the EDL. The 3CM is intrinsically symmetrical, but the MSM curve shows clear asymmetries.

dx.doi.org/10.1021/ct4002043 | J. Chem. Theory Comput. XXXX, XXX, XXX−XXX

of the material between the measurement location and the reference). Here, the electric surface potential is defined to be the electric potential measured at the fluid-wall interface, relative to a specified reference location, which we have chosen as our bulk fluid. It will be pointed out later that our bulk is a good choice for the reference potential.

The asymmetry of the MSM solvent creates an asymmetric surface potential trend, which can not be reproduced by the 3CM. Ironically, for low, negative surface charges, the MSM yields a positive potential. This is due to a number of factors, including but not limited to (i) the choice of measurement plane, (ii) the short distance between the wall and hydrogen atoms (from adsorbed water molecules), (iii) the small slope of the electric potential, and (iv) the relatively large amount of water molecules (compared to adsorbed counterions), which causes the hydrogen atoms to locally overscreen the applied electric field. Given that the inverse of the ζ versus σ curve is not a proper function, one should be cautioned when attempting to measure a capacitance.

While the applied surface charge is the same for both models, potentials are plotted on different scales because the electrostatic interactions are between 1 and 2 orders of magnitude different. In general, these results are in agreement with earlier theoretical and computational studies, which have shown that capacitances measured from primitive models (e.g., 3CM) can be greatly overpredicted due to mischaracterization of the dielectric response near interfaces.[57] The difference in magnitude of electric surface potential for the two models will be discussed in detail later.

Density Profiles. Figure 2 shows the density profiles for the 3CM cases on a linear scale. Due to the antisymmetry of the

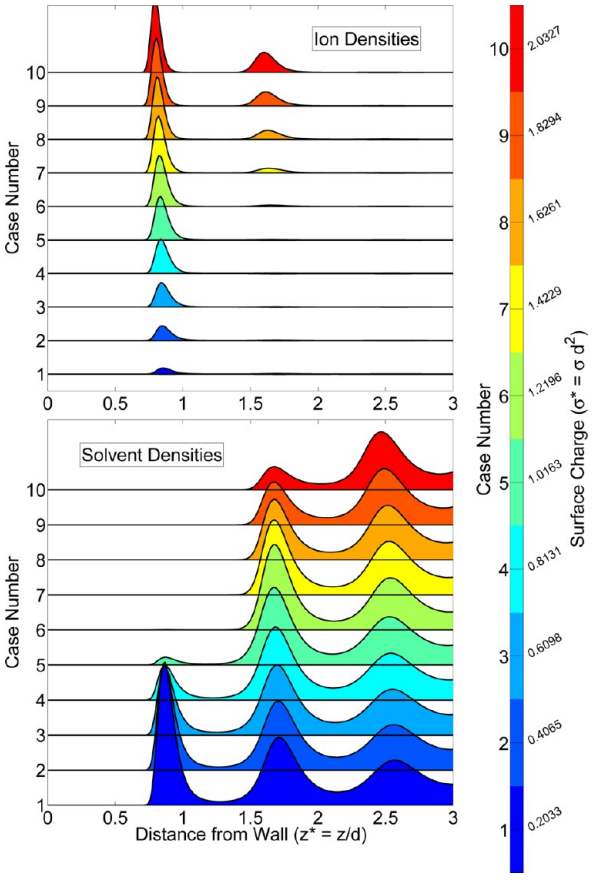

Figure 2. 3CM density profiles at 1 M and various surface charges. The upper plot is for the ion density, and the lower plot is for the solvent density. For the ion densities here, counterion densities are plotted as positive values, and coion densities are plotted as negative values. Each surface charge case is plotted at a different offset for comparison purposes.

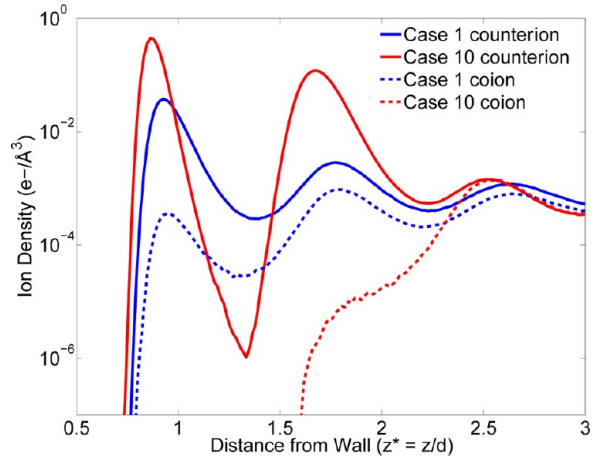

Figure 3. Highlight of ion density profiles for two 3CM surface charge cases. Counterion profiles are drawn with solid lines, and dashed lines represent coion profiles. Profiles are plotted on a logarithmic scale to show the relative behavior between the two ion types. Case 1 corresponds to a normalized surface charge of $\sigma^* = 0.2033$, and case 10 has a surface charge of $\sigma^* = 2.0327$.

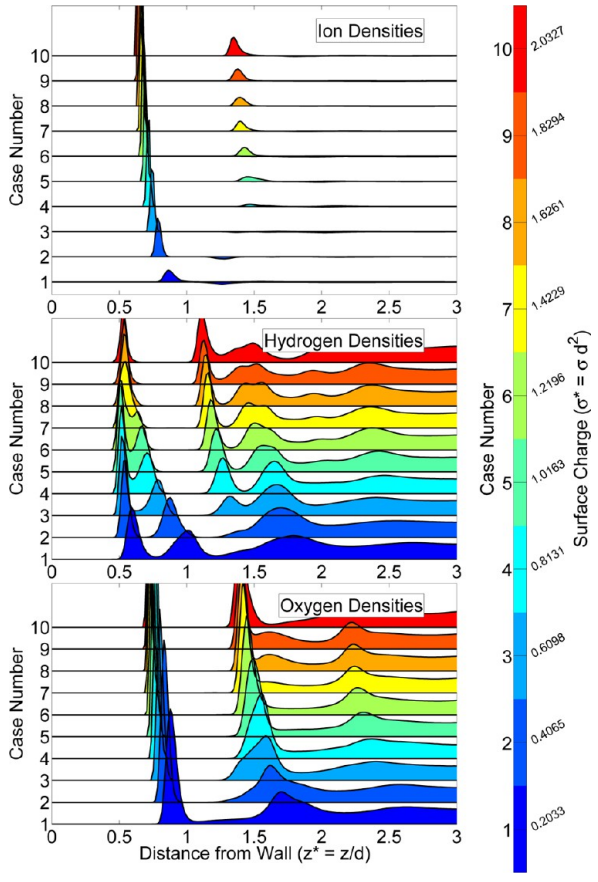

Figure 4. MSM density profiles at 1 M and various negative surface charges. For the ion densities here, counterion densities are plotted as positive values and coion densities are plotted as negative values. Each surface charge case is plotted at a different offset for comparison purposes.

dx.doi.org/10.1021/ct4002043 | J. Chem. Theory Comput. XXXX, XXX, XXX−XXX

model, only one wall is shown. The zero x-axis position in subsequent profile plots indicates the origin of the LJ wall. For discussion sake, we will label the cases 1 to 10, starting from the lowest surface charge case (consistent with axes labels in the figures). In accordance with observations by Lee et al.,[8] formation of the second counterion peak coincides with depletion of the solvent in the first peak position. Also, as surface charge increases, the ion peak shifts moderately toward the wall because surface repulsion is a soft-core interaction. Figure 3 highlights cases 1 and 10 on a logarithmic scale as examples. One can see from the log plot that the counterion density is always greater than or equal to the coion density at all locations in the double layer, consistent with PB theory.

Figures 4 and 5 show the density for the MSM results, both on a linear scale. Here, the left and right surfaces are plotted independently because of the asymmetry. Solvent density is split into two plots for the hydrogen and oxygen components. In the MSM, ions also shift closer to the surface as surface

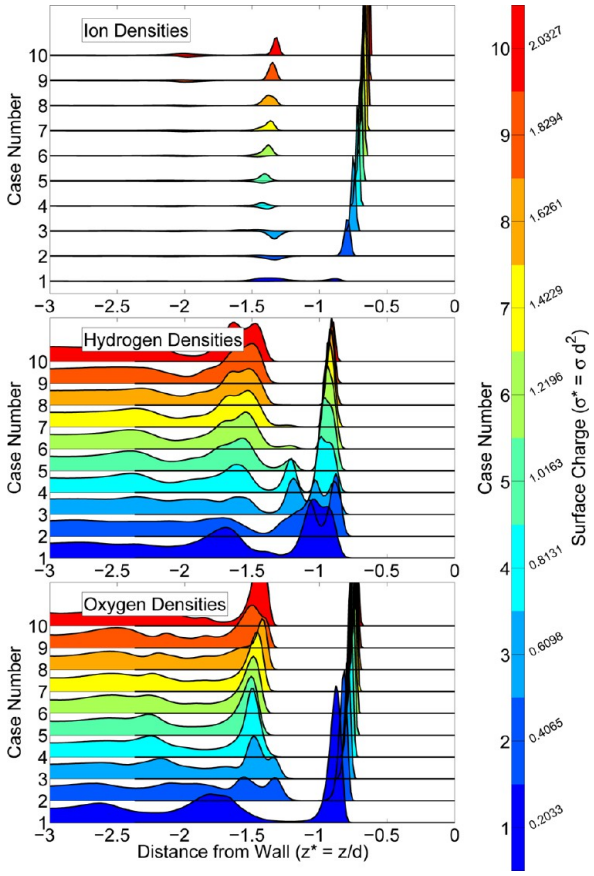

Figure 5. MSM density profiles at 1 M and various positive surface charges. For the ion densities here, counterion densities are plotted as positive values and coion densities are plotted as negative values. Each surface charge case is plotted at a different offset for comparison purposes.

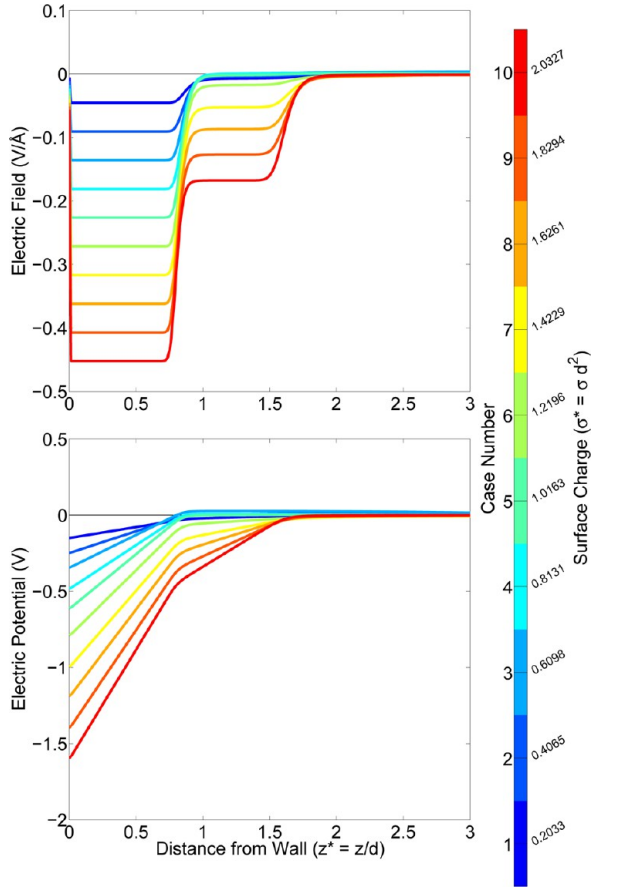

Figure 7. 3CM electric field and electric potential profiles at 1 M and various surface charges.

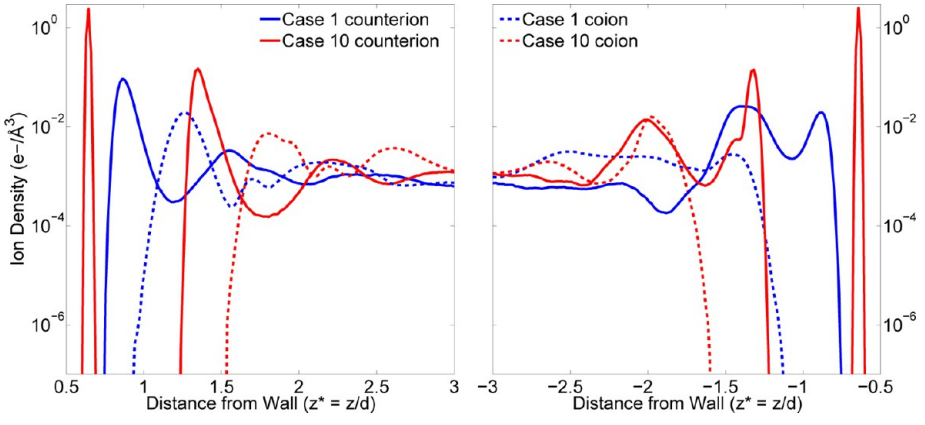

Figure 6. Highlight of MSM ion density profiles for two surface charge cases, corresponding to Figure 3. Cases 1 and 10 have normalized surface charges of $\sigma^* = 0.2033$ and 2.0327, respectively. Here, solid and dashed lines represent counterion and coion profiles, respectively. Profiles are plotted on a logarithmic scale to show the relative behavior between the two ion types.

dx.doi.org/10.1021/ct4002043 | J. Chem. Theory Comput. XXXX, XXX, XXX−XXX

charge increases, but much more noticeably than in the 3CM case. It appears to have asymptoted to its limit in the highest surface charge case. The decreased distance to the wall is magnified in the MSM case, at least in part due to the increased electrostatic interactions; recall that the 3CM interactions are weakened by a factor of 80, whereas the MSM interactions are only effectively weakened in the presence of solvation shells. With the MSM, not only does the wall partially disrupt solvation shells but also solvent near the wall has the tendency to align with the applied field rather than solvating nearby ions. Moreover, within the double layer, polarizability of the solvent is not necessarily equivalent to a relative permittivity value of 80, as this number applies specifically to bulk water.[58,59] Interestingly, as ions shift toward the surface, solvent also shifts with them; this phenomenon is not observed in the 3CM. It is perhaps due to the electrostatic interactions between the surface and the solvent being present in the MSM but not the 3CM. Also interesting is that complete solvent depletion is not observed in these MSM simulations, despite formation of the second ion layer.

Solvent behavior is particularly interesting. For negatively charged surfaces (Figure 4), the alignment of the water molecule shifts significantly as surface charge is increased. Strictly looking at the first layer of atoms, the dipoles from the low surface charge curves are only slightly oriented toward the surface. This can be seen from the first two hydrogen peaks (asymmetrically) straddling the first oxygen peak. By the highest surface charge, the hydrogen peaks have consolidated into one, which suggests the dipole vector is pointing directly toward the wall.

On the other hand, Figure 5 shows that the positively charged surface behaves differently. The first two or three cases show a very slightly off-axis dipole vector, but otherwise, the water molecule maintains approximately the same orientation for all surface charges. Curiously, only a few intermediate surface charge cases (i.e., cases 2−4) show a straddled water molecule in the second layer, but this feature is not observed in the second layer for higher or lower surface charges.

The density of MSM counterions and coions for two surface charge cases corresponding to those in Figure 3 are plotted on a logarithmic scale in Figure 6. The negatively charged wall (left) and positively charged wall (right) are shown side-by-side for comparison. The curves contain many more features than were observed in the corresponding 3CM plot, but the most important aspect to note is the criss-crossing ion density profiles, implying regions where coion presence can exceed counterion density. In all surface charge cases, the coion curves can be found to exceed the counterion density in some region in the condensed layer. This is markedly different than predictions from PB theory and the 3CM.

Electric Field and Electric Potential Profiles. In Figure 7, wall-normal electric field and electric potential profiles are shown for the 3CM cases. The wall-normal electric field component is calculated by integrating the net charge density. In turn, the electric potential is computed by integration of the electric field. The tiered electric field plot indicates that there is a maximum screening charge per layer. When the surface charge exceeds that limit, the second layer of ions begins to form. The turning point is case 5, where, in between the first and second layers, cases with normalized surface charges less than or equal to 0.9922 have a near zero electric field, and all higher surface charge cases have a significant residual electric field. This case corresponds to (i) the

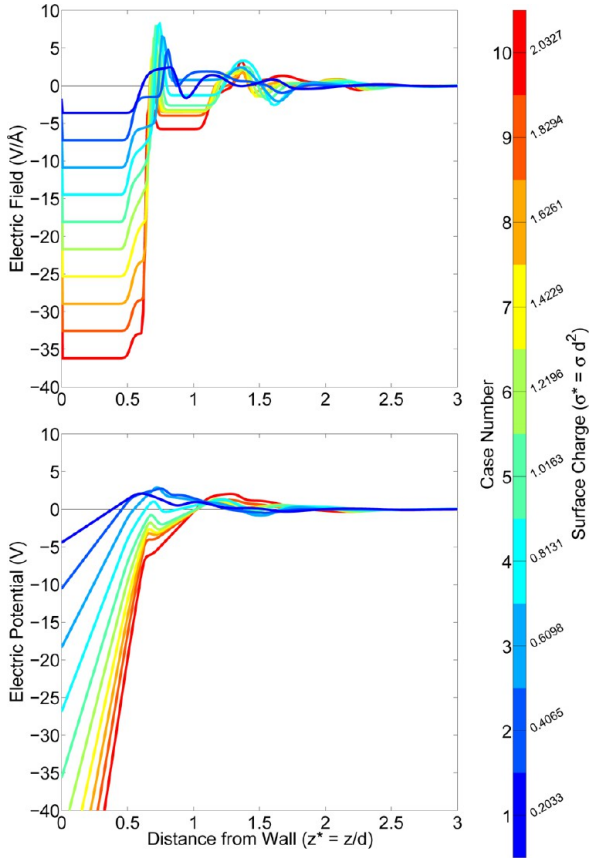

Figure 8. MSM electric field and electric potential profiles at 1 M and various negative surface charges.

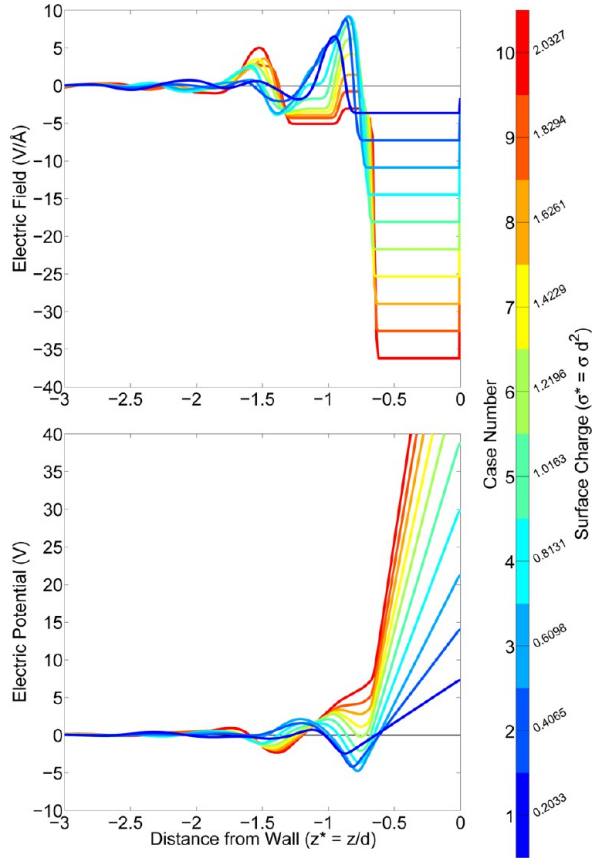

Figure 9. MSM electric field and electric potential profiles at 1 M and various positive surface charges.

dx.doi.org/10.1021/ct4002043 | J. Chem. Theory Comput. XXXX, XXX, XXX−XXX

inflection point in Figure 1, (ii) the onset of a second ionic screening layer, and (iii) the complete depletion of first solvent layer in Figure 2. For those higher surface charge cases, the electric field in the second layer increases linearly with the applied surface charge. Moreover, the incremental applied electric field from case to case is nearly equivalent to the change in the resulting electric field of the second layer.

The trends are not as simple in the MSM cases, shown in Figures 8 and 9. The electric field frequently changes signs due to the staggered positive and negative charges of the polar solvent. This causes local regions of over- and under-screening. In contrast to the 3CM results, screening in the second layer does not proceed linearly with the MSM. Even up to the highest surface charge case, a significant fraction of the applied field is screened within the first layer.

Note that both the electric fields and electric potentials from the MSM (Figures 8 and 9) differ by orders of magnitude compared to their counterparts in the 3CM (Figure 7). This difference in magnitude between the two models is important and is explained below. Recall that the electric surface potential is measured at one-half atomic diameter away from the LJ 10−4−3 wall origin, that is, 0.5 or −0.5 in the profile plots (Figures 2−9). Let us assume that the applied field is entirely screened by ions in the first layer, as shown in Figure 10. The electric field between the first layer and the surface then is nothing but the applied electric field, modulo a factor of the relative permittivity. Therefore, assuming the screening ions are all equidistant from the wall, we expect the electric surface potentials of the two models plotted in Figure 1 to differ by a factor of 80. However, the factor is found to asymptote to approximately 20. To explain this difference, it should be noted that the magnitude of the electric surface potential will depend upon the exact position of the first screening layer. In the 3CM (Figure 2), the first peaks are all approximately 0.9 molecular diameters from the wall. However, the ionic cores of the MSM range from 0.9 down to 0.6 molecular diameters. As depicted in Figure 10b, where the screening distance is adjusted, the measured electric surface potential will vary approximately linearly with the adjustment. Given that most of the MSM screening occurs 75% closer to the measurement point than the 3CM screening, the slope does not rise over the same distance, and the difference in scale is approximately 25% of the first order approximation, hence the factor of 20. At lower surface charges where the screening distance is similar to that of the 3CM, there is an interplay of more complex effects with the polar solvent that results in a range of scaling factors. Note also that the factor of 20 is unique to the choice of measurement plane.

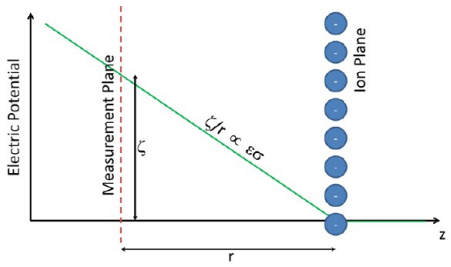

(a) Surface potential from first order approximation.

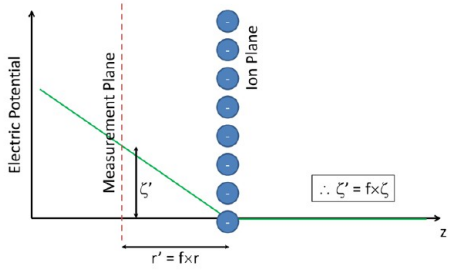

(b) Surface potential given a fraction f of the approach distance.

Figure 10. Diagrams depicting a first order approximation for calculating the electric surface potential. Ions are assumed to have infinite screening capability, thereby making the surface potential only a function of the applied charge and the distance between the measurement and screening planes.

REPEATED STRUCTURES

In the 3CM results, patterns in the first adsorbed layer for cases 1−4 are observed to repeat in the second layer for cases 7−10, respectively. For example, the applied electric field (see Figure 7) in case 1 is approximately equal to the residual electric field between the first and second layers of case 7. Similar observations can be made for subsequent cases in a one-to-one corresondence, that is, case 2 to case 8, case 3 to case 9, and case 4 to case 10.

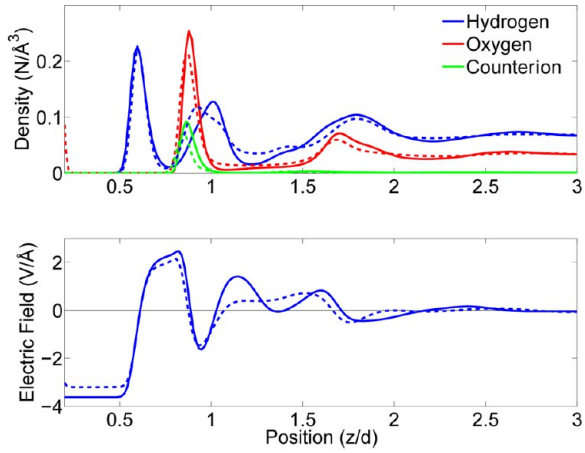

(a) Case 1 first layer (solid lines) vs. Case 6 second layer (dashed lines)

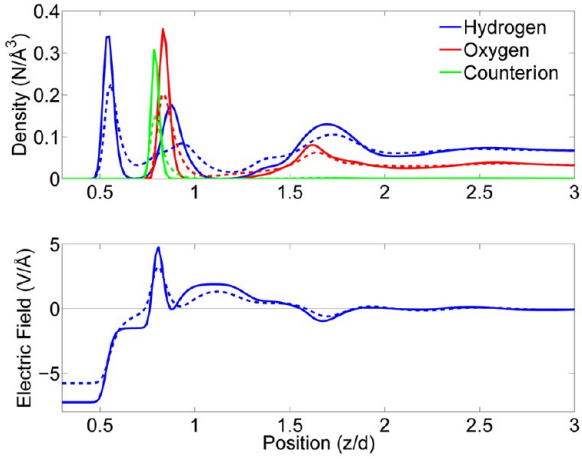

(b) Case 2 first layer (solid lines) vs. Case 10 second layer (dashed lines)

Figure 11. MSM at the negatively charged surface is observed to repeat first layer behavior for low surface charge cases to second layer behavior for higher surface charge cases, but the repetition does not occur linearly with applied surface charge. Second layer profiles are shifted horizontally to highlight the comparison.

dx.doi.org/10.1021/ct4002043 | J. Chem. Theory Comput. XXXX, XXX, XXX−XXX

Moreover, not only do the patterns repeat for the electric field, but the electric potential (Figure 7) and density (Figure 2) profiles also show similar repetitions. We conjecture that the structures in the 3CM are repeated as manifest from the value of the local electric fields.

However, repetitions are not manifested in the same way in the MSM. For case 1 at the negatively charged wall, the solvent structure in the first layer strongly resembles the solvent structure in the second layer of case 6 (see Figure 4). Similarly, as seen in Figure 8, the applied electric field in case 1 is almost equivalent to the residual electric field between the first and second layers of case 6. Unlike the 3CM however, there is not a one-to-one correspondence for subsequent cases. Instead, similar observations (for the negatively charged wall) are made with cases 2 and 10. The repeated patterns are highlighted in Figure 11a and b, where the densities and electric fields of cases 1 and 2 are overlaid on those of cases 6 and 10, respectively.

First to second layer comparisons were not nearly as good for MSM cases at the positively charged wall. While the applied field in case 1 is similar to the unscreened field between the first and second layers of cases 5−10 (see Figure 9), the density and electric field profiles do not look similar. Water orientation is considerably different in the low charge regime (which we will explore in depth later). A number of factors presumably combine to disrupt the repetition of structure, at least for low surface charges. It is unclear what would happen at higher surface charges, as our case 2 has a larger first layer counterion peak than any second layer counterion peak of subsequent cases. The applied electric field is also greater than any resultant field of any other case. Even larger surface charges need to be simulated in order to definitively make the comparison.

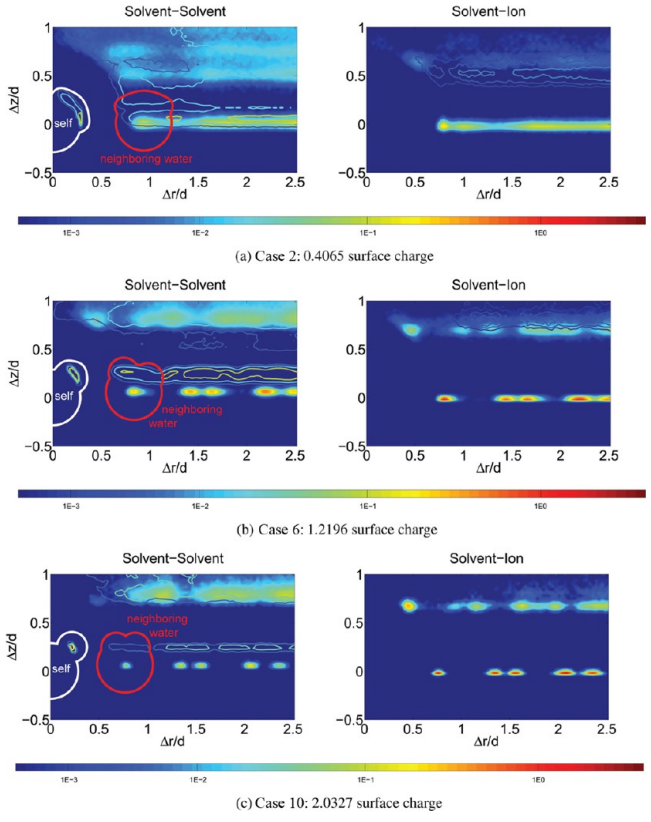

Figure 12. Correlation function contours in cylindrical coordinates, referenced against an oxygen atom in the first adsorbed layer at the positively charged wall for the MSM. In solvent−solvent plots, hydrogen correlations are plotted as unfilled contours, and oxygen correlations are plotted as filled contours. The reference and neighboring water molecules are highlighted with thick white and red outlines, respectively. In solvent−ion plots, coion correlations are plotted as unfilled contours and counterion correlations are plotted as filled contours.

Correlation Functions. To understand the structure of the double layer, we computed various correlation functions for the MSM. We developed our own correlation functions, inspired by the radial distribution function, using cylindrical coordinates. Given a reference atom (either a counterion or oxygen atom) in the first adsorbed layer, the correlation function describes how densities of other atoms vary as functions of radial and longitudinal distance away from the reference atom. The radial distance, Δr, is in the plane parallel to the wall, and the longitudinal distance, Δz, is perpendicular to the wall. Figures 12−15 plot these correlation functions as contours for a range of surface charges. Figures 12 and 13 correspond to the reference atom being an oxygen atom near positively and negatively charged walls, respectively. Likewise, Figures 14 and 15 correspond to the reference atom being a counterion near positive and negative walls, respectively. It is clear from the figures how the wall causes the fluid to take on a solid-like structure. There are clearly defined layers nearest to the wall, corresponding to the peaks of Figures 4 and 5. While the axis limits

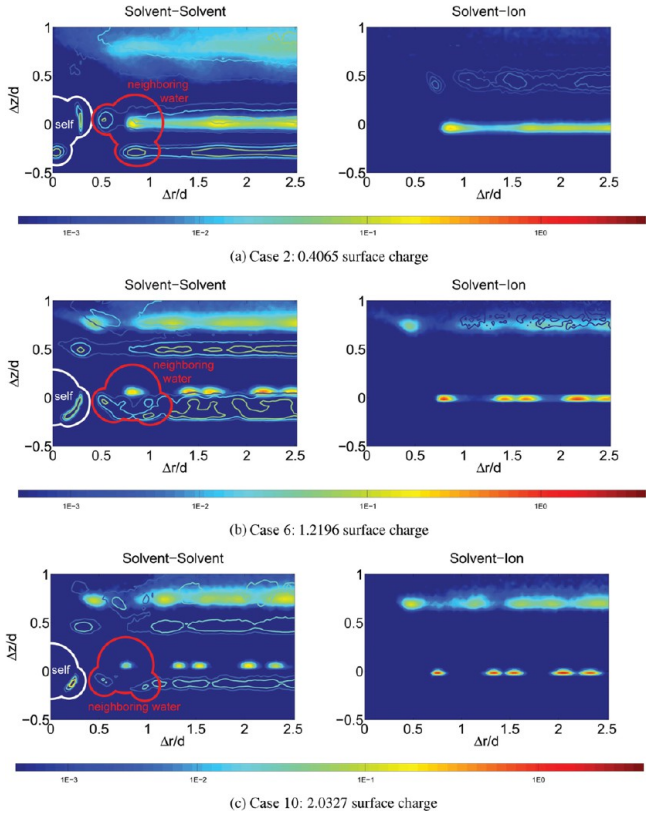

Figure 13. Correlation function contours in cylindrical coordinates, referenced against an oxygen atom in the first adsorbed layer at the negatively charged wall for the MSM. In solvent−solvent plots, hydrogen correlations are plotted as unfilled contours, and oxygen correlations are plotted as filled contours. The reference and neighboring water molecules are highlighted with thick white and red outlines, respectively. In solvent−ion plots, coion correlations are plotted as unfilled contours and counterion correlations are plotted as filled contours.

dx.doi.org/10.1021/ct4002043 | J. Chem. Theory Comput. XXXX, XXX, XXX−XXX

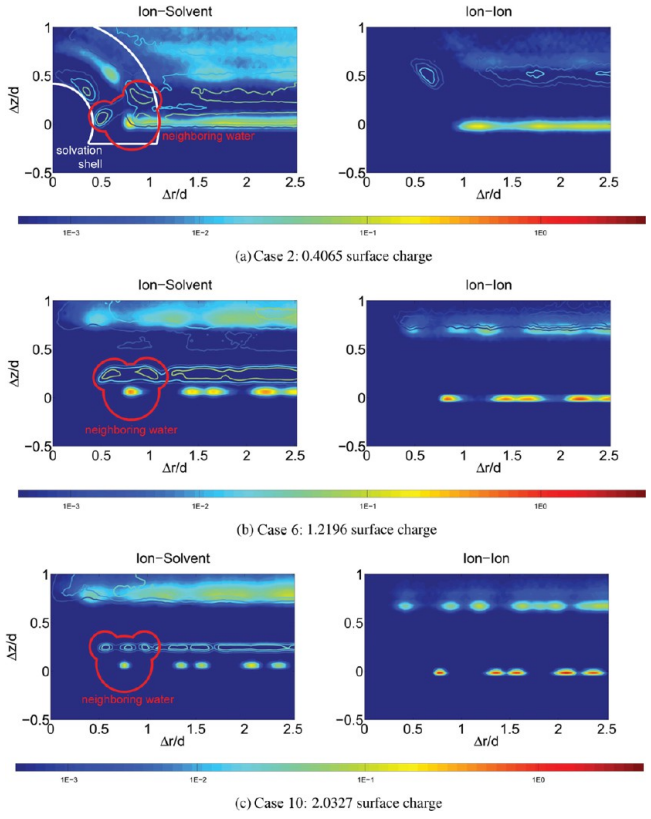

Figure 14. Correlation function contours in cylindrical coordinates, referenced against a counterion in the first adsorbed layer at the positively charged wall for the MSM. In solvent–solvent plots, hydrogen correlations are plotted as unfilled contours, and oxygen correlations are plotted as filled contours. The neighboring water molecule is highlighted with a thick red outline, and a solvation shell is highlighted in white, when visible. In solvent–ion plots, coion correlations are plotted as unfilled contours and counterion correlations are plotted as filled contours.

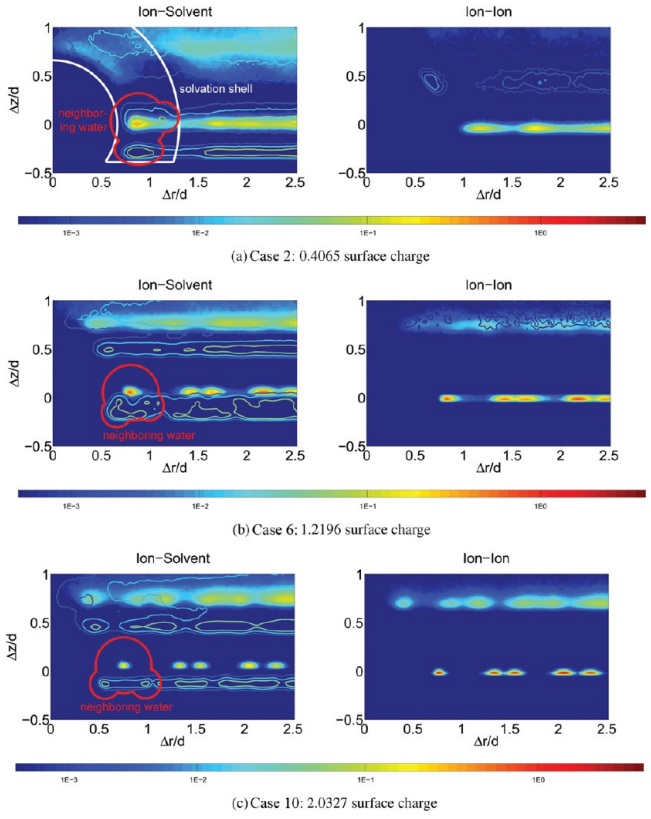

Figure 15. Correlation function contours in cylindrical coordinates, referenced against a counterion in the first adsorbed layer at the negatively charged wall for the MSM. In solvent–solvent plots, hydrogen correlations are plotted as unfilled contours, and oxygen correlations are plotted as filled contours. The neighboring water molecule is highlighted with a thick red outline, and a solvation shell is highlighted in white, when visible. In solvent–ion plots, coion correlations are plotted as unfilled contours and counterion correlations are plotted as filled contours.

of the plots are small to highlight local features, the correlation function does become smeared as Δz approaches the bulk. Moreover, the adsorbed layer becomes highly structured with increasing surface charge; that is, the oxygen and ion contours in the first layer tend toward distinct peaks as surface charge increases. These peaks also tend to blur into one another with increasing Δr, as is expected even with perfect lattices.

As seen in the solvent–solvent plots of Figure 12, the orientations of the reference and neighboring water molecules remain approximately consistent through all surface charges, albeit a tightening of their positions. Conversely, for the negatively charged wall, the orientation of the water molecule in the adsorbed layer has a clear shift. Under low surface charges (Figure 13a), one hydrogen plane is slightly above the oxygen plane, while the other hydrogen atom points approximately toward the wall. As surface charge increases (Figure 13b and c), the molecule rotates so that both hydrogen atoms are equidistant from the surface. As a sidenote, the reference and neighboring water molecules in Figure 13a may look peculiar because there are seemingly two hydrogen atoms adjacent to one another. Due to the cylindrical averaging scheme, the *x*- and *y*-dimensions are collapsed onto a single axis, so in real space the hydrogen atoms are not actually adjacent. In fact, visualization of the simulation reveals a chain-like network of hydrogen bonds for low surface charges, similar to other observations of water in confined spaces.[60]

In Figure 14, where the surface is positively charged and the reference atom is a negative ion, the neighboring water molecule is turned slightly toward the reference counterion under low surface charge. In this regime, the hydrogen atom is affected by the presence of the counterion as well as the applied electric field. Since the dipole vector is slightly aligned toward the ion, the water molecule is partially solvating the ion. Hypothetically, a radial distribution function for a fully solvated ion in bulk fluid would be indistinguishable from a distribution function which includes angular or longitudinal dependency because of isotropy. Therefore, any correlation function contour uniformly smeared in a circular shape may be approximately interpreted as a solvation shell. As such, a solvation shell can be inferred from the low charge case of Figure 14, especially beyond the first layer. As the surface charge increases, the influence of the counterion becomes weaker relative to the wall charge, and the dipole vector points normal to the surface. In these latter cases, the water no longer acts as a solvent, and the solvation shell is not as clearly discernible. At the negatively charged wall (Figure 15), the neighboring water molecule undergoes the same rotation as shown in Figure 13, except the dipole vector initially points slightly away from the reference atom. Here, the solvation shell is slightly larger than for the negative ion since the hydrogens point outward. Again, under low charge, neighboring atoms affect the water orientation; however, the effect of the local distrubtion of atoms becomes negligible under higher

dx.doi.org/10.1021/ct4002043 | J. Chem. Theory Comput. XXXX, XXX, XXX–XXX

surface charges. The shell is also not easily discernible for higher charge cases at the negatively charged wall.

CONCLUSION

To better understand the EDL and the physics that affect it, we compared two different solvent models using MD simulation. The MSM explicitly models the atoms in the polar molecule (in this case, TIP3P water). On the other hand, the 3CM can be viewed as a coarse-grained approximation where the solvent is treated as a chargeless atom, and a uniform dielectric constant is used to account for the polar nature of solvating fluids. It was shown that the 3CM and the MSM produce ion densities that are qualitatively similar, but close inspection reveals subtle differences in positions. These subtle differences and details about the orientation of solvent molecules for the MSM greatly affect the quantitative measurements of electric fields, electric potentials, and capacitances. Near the wall, these quantities are shown to differ by an order of magnitude. Moreover, the MSM allows a larger amount of coions to exist in the EDL, to the point of exceeding counterion densities in some regions. This has not been observed in any 3CM study (past or present) or PB theory. Due to this phenomenon and other complex effects in the MSM, the electric field and electric potential are observed to overshoot the requisite screening, and decaying oscillations bring them to bulk conditions.

Density, electric field, and electric potential patterns are observed in the 3CM to repeat from one layer to the next for different surface charge cases. This happens when the first ionic layer screens away enough electric field to match the applied electric field of a lower surface charge case. Also in the 3CM, the residual electric field between the first and second layers linearly increases with the applied charge. However, in the MSM, repetitions do not occur linearly nor do they advance in an equivalent manner as the applied charge increases. Moreover, these repetitions are observed only at the negatively charged surface. We also presented correlation function contour plots that reveal water molecule reorientation effects and oscillations of coion and counterion charge. The reorientation of water indicates that the water's tendency to solvate ions near the wall is effectively nullified under high surface charges, thus having the direct consequence of altering the permittivity. In the Supporting Information, we also show quantitatively that the structure of the adsorbed layers is similar between the two models, but with some key differences attributable to a combination of the dielectric constant and coion presence.

ASSOCIATED CONTENT

Supporting Information

Additional text and figure showing centrosymmetry of the first two adsorbed layers. This material is available free of charge via the Internet at http://pubs.acs.org.

AUTHOR INFORMATION

Corresponding Author

*E-mail: jatempl@sandia.gov.

Notes

The authors declare no competing financial interest.

ACKNOWLEDGMENTS

The authors would like to thank Reese Jones for helpful conversations. Sandia National Laboratories is a multiprogram laboratory managed and operated by Sandia Corporation, a wholly owned subsidiary of Lockheed Martin Corporation, for the U.S. Department of Energy's National Nuclear Security Administration under Contract No. DE-AC04-94AL85000. Funding for this work was provided by the Laboratory Directed Research and Development program at Sandia National Laboratories, and its support is gratefully acknowledged.

REFERENCES

(1) Conway, B. *J. Electrochem. Soc.* **1991**, *138*, 1539−1548.
(2) Conway, B. E. *Electrochemical Supercapacitors*; Kulwer Academic: New York, 1999.
(3) Harnett, C. K.; Templeton, J.; Dunphy-Guzman, K. A.; Senousy, Y. M.; Kanouff, M. P. *Lab Chip* **2008**, *8*, 565−572.
(4) Srinivasan, S., *Bioelectrochemistry*; Springer: New York, 1985; Vol. *10*.
(5) Sjöström, L.; Akesson, T.; Jönsson, B. *Ber. Bunsen-Ges. Phys. Chem.* **1996**, *100*, 889−893.
(6) Hunter, R. J. *Foundations of Colloid Science*, 2nd ed.; Oxford University Press: Oxford, 2000.
(7) Nilson, R. H.; Griffiths, S. K. *J. Chem. Phys.* **2006**, *125* (16), 164510.
(8) Lee, J. W.; Nilson, R. H.; Templeton, J. A.; Griffiths, S. K.; Kung, A.; Wong, B. M. *J. Chem. Theory Comput.* **2012**, *8*, 2012−2022.
(9) Dani, J. *Biophys. J.* **1986**, *49*, 607−618.
(10) Adcock, C.; Smith, G. R.; Sansom, M. S. P. *Biophys. J.* **1998**, *75*, 1211−1222.
(11) Rostovtseva, T. K.; Aguilella, V. M.; Vodyanoy, I.; Bezrukov, S. M.; Parsegian, V. A. *Biophys. J.* **1998**, *75*, 1783−1792.
(12) Freund, J. B. *J. Chem. Phys.* **2002**, *116*, 2194−2200.
(13) Qiao, R.; Aluru, N. R. *J. Chem. Phys.* **2003**, *118*, 4692−4701.
(14) Stein, D.; Kruithof, M.; Dekker, C. *Phys. Rev. Lett.* **2004**, *93*, .
(15) Kim, D.; Darve, E. *Phys. Rev. E* **2006**, *73*, 051203.
(16) Eigen, M.; Wicke, E. *J. Phys. Chem.* **1954**, *58*, 702−714.
(17) Kralj-Iglic, V.; Iglic, A. *J. Phys. II France* **1996**, *6*, 477−491.
(18) Lamperski, S.; Outhwaite, C. W.; Bhuiyan, L. B. *Mol. Phys.* **1996**, *87*, 1049−1061.
(19) Borukhov, I.; Andelman, D.; Orland, H. *Phys. Rev. Lett.* **1997**, *79*, 435−438.
(20) Fedorov, M. V.; Kornyshev, A. A. *Electrochim. Acta* **2008**, *53*, 6835−6840.
(21) Wang, H.; Pilon, L. *J. Phys. Chem. C* **2011**, *115*, 16711−16719.
(22) Tang, Z.; Scriven, L. E.; Davis, H. T. *J. Chem. Phys.* **1992**, *97*, 494−503.
(23) Henderson, D.; Jiang, D.; Jin, Z.; Wu, J. *J. Phys. Chem. B* **2012**, *116*, 11356−11361.
(24) Plischke, M.; Henderson, D. *J. Chem. Phys.* **1988**, *90*, 5738−5741.
(25) Tang, Z. X.; Mier-y-Teran, L.; Davis, H. T.; Scriven, L. E.; White, H. S. *Mol. Phys.* **1990**, *71*, 369−392.
(26) Torrie, G. M.; Valleau, J. P. *Chem. Phys. Lett.* **1979**, *65*, 343−346.
(27) Torrie, G. M.; Valleau, J. P. *J. Chem. Phys.* **1980**, *73*, 5807−5816.
(28) Torrie, G. M.; Valleau, J. P. *J. Phys. Chem.* **1982**, *86*, 3251−3257.
(29) Torrie, G. M.; Kusalik, P. G.; Patey, G. M. *J. Chem. Phys.* **1989**, *91*, 6367−6375.
(30) Lamperski, S.; Bhuiyan, L. B. *J. Electroanal. Chem.* **2003**, *540*, 79−87.
(31) Lamperski, S.; Zydor, A. *Electrochim. Acta* **2007**, *52*, 2429−2436.
(32) Kilic, M. S.; Bazant, M. Z.; Ajdari, A. *Phys. Rev. E* **2007**, *75*, 021502.
(33) Spohr, E. *Electrochim. Acta* **1999**, *44*, 1697−1705.
(34) Crozier, P. S.; Rowley, R. L.; Spohr, E.; Henderson, D. *J. Chem. Phys.* **2000**, *112*, 9253−9257.
(35) Thompson, A. P. *J. Chem. Phys.* **2003**, *119*, 7503−7511.
(36) Qiao, R.; Aluru, N. R. *Phys. Rev. Lett.* **2004**, *92*, 198301.
(37) Xu, D.; Li, D.; Leng, Y.; Chen, Y. *Mol. Sim.* **2007**, *33*, 959−963.
(38) Willard, A. P.; Reed, S. K.; Madden, P. A.; Chandler, D. *Faraday Discuss.* **2009**, *141*, 423−441.

(39) Feng, G.; Qiao, R.; Huang, J.; Sumpter, B. G.; Meunier, V. *ACS Nano* **2010**, *4*, 2382−2390.
(40) Wu, P.; Qiao, R. *Phys. Fluids* **2011**, *23*, .
(41) Plimpton, S. J. *J. Comput. Phys.* **1995**, *117*, 1−19.
(42) Jorgensen, W. L.; Chandrasekhar, J.; Madura, J. D.; Impey, R. W.; Klein, M. L. *J. Chem. Phys.* **1983**, *79*, 926−935.
(43) Price, D. J.; Brooks, C. L. *J. Chem. Phys.* **2004**, *121*, 10096−10103.
(44) Jones, J. E. *Proc. R. Soc. A* **1924**, *106*, 436−477.
(45) Ryckaert, J.-P.; Ciccotti, G.; Berendsen, H. J. C. *J. Comput. Phys.* **1977**, *23*, 327−341.
(46) Magda, J. J.; Tirrell, M.; Davis, H. T. *J. Chem. Phys.* **1985**, *83*, 1888−1901.
(47) Verlet, L. *Phys. Rev.* **1967**, *159*, 98−103.
(48) Verlet, L. *Phys. Rev.* **1968**, *165*, 201−214.
(49) Hockney, R. W.; Eastwood, J. W. *Computer Simulation Using Particles*; Taylor and Francis: New York, 1989.
(50) Yeh, I.-C.; Berkowitz, M. L. *J. Chem. Phys.* **1999**, *111*, 3155−3162.
(51) Lorentz, H. A. *Ann. Phys.* **1881**, *248*, 127−136.
(52) Berthelot, D. *C. R. Hebd. Séances Acad. Sci.* **1898**, *126*, 1703−1855.
(53) Nosé, S. *J. Chem. Phys.* **1984**, *81*, 511−519.
(54) Hoover, W. G. *Phys. Rev. A* **1985**, *31*, 1695−1697.
(55) Martyna, G. J.; Klein, M. L.; Tuckerman, M. *J. Chem. Phys.* **1992**, *97*, 2635−2643.
(56) Zimmerman, J. A.; Webb, E. B., III; Hoyt, J. J.; Jones, R. E.; Klein, P. A.; Bammann, D. J. *Modell. Simul. Mater. Sci. Eng.* **2004**, *12*, S319−S332.
(57) Blum, L.; Henderson, D. *J. Chem. Phys.* **1981**, *43*, 1901−1910.
(58) MacDonald, J. R. *J. Electroanal. Chem.* **1987**, *223*, 1−23.
(59) Bonthuis, D. J.; Gekle, S.; Netz, R. R. *Phys. Rev. Lett.* **2011**, *107*, 166102.
(60) Yuan, Q.; Zhao, Y.-P. *J. Am. Chem. Soc.* **2009**, *131*, 6374−6376.